Time-reversal symmetry breaking and multigap superconductivity in the noncentrosymmetric superconductor La$_7$Ni$_3$

Arushi,[1] D. Singh,[2] A. D. Hillier [2] M. S. Scheurer,[3] and R. P. Singh [1,*]

[1]*Department of Physics, Indian Institute of Science Education and Research Bhopal, Bhopal, 462066, India*
[2]*ISIS Facility, STFC Rutherford Appleton Laboratory, Didcot OX11 0QX, United Kingdom*
[3]*Institute for Theoretical Physics, University of Innsbruck, A-6020 Innsbruck, Austria*

The Th$_7$Fe$_3$ family of superconductors provides a rich playground for unconventional superconductivity. La$_7$Ni$_3$ is the latest member of this family, which we here investigate by means of thermodynamic and muon spin rotation and relaxation measurements. Our specific heat data provides evidence for two distinct and approximately isotropic superconducting gaps. The larger gap has a value slightly higher than that of weak-coupling BCS theory, indicating the presence of significant correlations. These observations are confirmed by transverse-field muon spin rotation/relaxation measurements. Furthermore, zero-field measurements reveal small internal fields in the superconducting state, which occur close to the onset of superconductivity and indicate that the superconducting order parameter breaks time-reversal symmetry. We discuss two possible microscopic scenarios—an unconventional $E_2(1, i)$ state and an $s + i s$ superconductor, which is reached by two consecutive transitions—and illustrate which interactions will favor these phases. Our results establish La$_7$Ni$_3$ as the first member of the Th$_7$Fe$_3$ family displaying both time-reversal-symmetry-breaking and multigap superconductivity.

I. INTRODUCTION

While the superconducting transition of the original Bardeen-Cooper-Schrieffer (BCS) theory is not a symmetry-breaking phase transition but rather a condensed-matter realization of a Higgs mechanism [1,2], modern research in superconductivity is crucially concerned with the aspect of symmetry [3,4]: First, the superconducting order parameter might transform nontrivially under a subgroup of the symmetries of the normal state. In that case, the superconducting transition is also a symmetry-breaking phase transition. Second, a lot of research is concerned with the realization and study of superconductivity in systems with reduced symmetries, driven by the goal of designing superconductors with exotic and potentially useful properties. Among these, noncentrosymmetric crystal structures with significant spin-orbit coupling are of particular interest [4]; they exhibit inversion antisymmetric Rashba-Dresselhaus spin-orbit-coupling terms [5,6], which result in the splitting of the Fermi surfaces into two opposite spin configurations. This has a pronounced effect on the possible pairing states and leads to mixed-parity spin states (singlet and triplet) in the order parameter [4,7–9]. As a result, it can give rise to some novel and uncommon superconducting properties, such as unusually high upper critical fields, larger than the Pauli limit [8,10–13], the presence of nontrivial line or point nodes [14–18], multiple-gap behavior [12,19], an enhanced protection against impurity scattering [20–27], and the more recently proposed topological superconductivity [28–33].

One of the most fascinating and intensely studied cases of broken symmetries in the superconducting state is time-reversal-symmetry (TRS) breaking. This is not only due to the fact that TRS-breaking superconductors can exhibit topological chiral edge modes [28] but also by the fundamental role of TRS for superconductivity itself [34], which is associated with the formation of bound states of electrons at momenta related by time reversal. While a lot of weakly correlated noncentrosymmetric superconductors have been studied [35–38], TRS breaking has only been observed in a handful of them [10,39–46]. In general, the key ingredients for TRS breaking at a superconducting transition are mostly unknown, although some general constraints have recently been derived theoretically for spin-orbit-coupled noncentrosymmetric systems [47,48].

Noncentrosymmetric superconductivity in compounds with α-Mn structure (with or without Re concentration) has been examined a lot; however, indications of TRS breaking have only been observed for Re-based [Re$_6$X (X = Zr,Hf,Ti)] superconductors, where the strength of the internal field is found out to be almost equivalent for the mentioned alloys which suggests the contribution of Re in inducing TRS breaking in these systems [10,42–44]. Re's relevance is corroborated further by theoretical calculations [49] that suggest the dominance of the density of states of Re at the Fermi level. These observations indicate the vital role of Re together with the lack of inversion symmetry for the formation of superconductivity.

Similarly, the study of other noncentrosymmetric superconductors with a heavy element (other than Re) whose density of states at the Fermi level dominates can help us establish a relation between broken inversion symmetry and

*rpsingh@iiserb.ac.in

TRS of the superconductor, and the existence of a dominant density of states of a particular element in a compound. In this regard, the noncentrosymmetric superconducting family La_7X_3 (X = Ir, Rh, Ni), crystallizing in a Th_7Fe_3-type structure, which already shows examples of TRS breaking [45,50], provides potential candidates to investigate the above suggestions. In these cases also, the magnitude of the TRS-breaking signal remains approximately unchanged after replacing a $5d$ [La_7Ir_3] [45] by a $4d$ element [La_7Rh_3] [50], like in the Re_6X series compounds [10,42–44]. This may be due to the dominant role played by Re and La at the respective Fermi surfaces [49,51].

In this paper, the properties of La_7Ni_3, the youngest member of the La_7X_3 series, are analyzed using muon spin relaxation and rotation (μSR) supplemented by thermodynamic measurements. μSR in zero-field mode is one of the best-suited techniques for studying TRS breaking as it is susceptible to tiny changes in the internal fields ($\simeq 10\ \mu$T). Our zero-field measurements reveal the appearance of spontaneous internal magnetic fields in the superconducting state. This provides substantial evidence for broken TRS in La_7Ni_3, with a magnitude similar to La_7Ir_3 and La_7Rh_3. Generally, the spin-orbit coupling contribution from a $3d$ element, such as Ni, is considered negligible, which points towards the probable dominance of La in determining the superconducting ground state of La_7Ni_3. We further perform μSR measurements in the presence of a transverse magnetic field, which allows us to determine the temperature evolution of the magnetic penetration depth (λ) and, thus, infers additional information on the superconducting gap of La_7Ni_3.

The remainder of the paper is organized as follows: After presenting details on the sample preparation and measurement techniques in Sec. II, we show our specific heat and μSR data in Sec. III and how it was fitted. Section IV contains a discussion of possible microscopic pairing scenarios and of the role of disorder. A summary and outlook can be found in Sec. V. Two appendices provide details on how physical parameters are extracted from the data and discuss phenomenological models for the possible microscopic pairing scenarios.

II. EXPERIMENTAL DETAILS

The sample of La_7Ni_3 was prepared by arc melting stoichiometric amounts of La (99.9%) and Ni (99.95%) in a high purity argon gas atmosphere on a water-cooled copper hearth. The sample button was melted several times to ensure phase homogeneity with negligible weight loss (<1%). Magnetization and specific heat measurements were carried out using Quantum Design MPMS 3 and physical property measurement system (PPMS).

Muon-spin rotation and relaxation measurements were performed at the ISIS pulsed neutron and muon source, Rutherford Appleton Laboratory, the United Kingdom, in two different configurations (transverse, zero/longitudinal field). A detailed account on the μSR technique can be found in Ref. [52]. Three sets of orthogonal coils and an active compensation system are used to cancel the stray fields within 1 μT, which can be present at the sample position due to the Earth and neighboring instruments. La_7Ni_3 in powdered form was placed in a dilution refrigerator after mounting on a silver

TABLE I. Parameters obtained from various measurements.

Parameters	Units	La_7Ni_3	La_7Rh_3 [50]	La_7Ir_3 [84]
T_c	K	2.3	2.65	2.25
$H_{c1}(0)$	mT	5.19	2.51	3
$H_{c2}(0)$	T	0.71	1.02	0.97
$\xi_{GL}(0)$	Å	215	179	174
$\lambda_{GL}(0)$	Å	2940	4620	4720
κ_{GL}		26	26	21

holder, with diluted GE varnish operated in the temperature range 0.1 K $\leqslant$ T $\leqslant$ 3.0 K.

III. RESULTS

The powder x-ray diffraction (XRD) collected at room temperature, shown in Fig. 1(a), confirmed the crystal structure as hexagonal with space group $P6_3mc$ (No. 186). The lattice constants are: $a = b = 10.143 \pm 0.010$ Å and $c = 6.468 \pm 0.006$ Å which are in agreement with the previously published data [53]. From the magnetization measurements shown in Fig. 1(b) we find a superconducting transition temperature of $T_c = 2.3 \pm 0.1$ K, which also agrees with previously published results [54] and is found to be accompanied by a drop in resistivity (see Appendix A). The superconducting parameters coherence length, penetration depth, and critical fields of La_7Ni_3 have been extracted from our magnetization/susceptibility measurements and are summarized in Table I.

A. Specific heat

We have also measured the specific heat C and the normal state data was fitted with $C = \gamma_n T + \beta_3 T^3 + \beta_5 T^5$ where γ_n is the Sommerfeld constant representing the electronic contribution, and β_3, β_5 characterize the phononic contribution. The fit yields $\gamma_n = 44.43 \pm 0.84$ mJ mol^{-1} K^{-2}, $\beta_3 = 3.94 \pm 0.07$ mJ mol^{-1} K^{-4}, and $\beta_5 = 2.16 \pm 0.16$ μJ mol^{-1} K^{-6}. To extract the electronic part C_{el}, we subtracted the phononic contribution from the total heat capacity, $C_{el} = C - C_{ph} = C - \beta_3 T^3 - \beta_5 T^5$. C_{el}, normalized with respect to $\gamma_n T$, is shown in Fig. 1(c) as a function of reduced temperature, T/T_c. The data of C_{el} were fitted to the following models: (i) a single s-wave gap, which is taken to be isotropic and where $\alpha = \Delta(T=0)/k_B T_c$ is set to the BCS value, $\alpha = \alpha_{BCS} \simeq 1.764$; (ii) an isotropic s-wave gap with α as a variable parameter, also known as the α model [55]; (iii) a line-nodal d-wave gap; (iv) a phenomenological two-gap α model [56] with three fitting parameters—the values of $\alpha_j = \Delta_j(0)/k_B T_c$ of the two gaps, and x (with $0 \leqslant x \leqslant 0.5$ without loss of generality), which parameterizes the ratio of the partial Sommerfeld coefficients (or densities of states), $\gamma_1 = x\gamma_n$ and $\gamma_2 = (1-x)\gamma_n$, of the parts of the Fermi surface with gap values Δ_1 and Δ_2, respectively.

The resulting fits for the different models are shown in Fig. 1(c). We can clearly see that the medium- and low-temperature behavior is captured only by the two-gap model. Fitting yields $x = 0.23$, $\alpha_1 = 0.65$, and $\alpha_2 = 1.95$. We, thus, find a quite large difference in gap magnitude with ratio
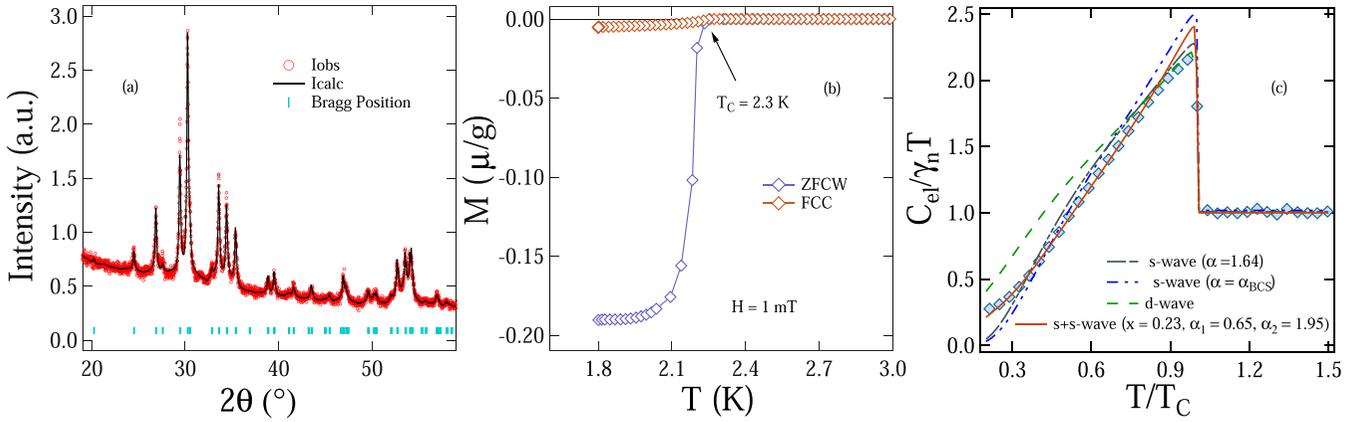
FIG. 1. (a) Powder XRD pattern of La_7Ni_3 is presented by red dots whereas the black line corresponds to the Rietveld refinement. (b) Magnetization as a function of temperature collected in the zero-field cooled warming (ZFCW) and field cooled cooling (FCC), confirming superconductivity with critical temperature $T_c = 2.3$ K. (c) Temperature dependence of normalized electronic specific heat data, where the dashed and solid lines represent fits to the different models described in the main text.

$\Delta_2(0)/\Delta_1(0) \simeq 3$. As expected, the relative weight of the smaller gap is suppressed, $x : (1 - x) \simeq 23\% : 77\%$. The value of α_2, which represents the larger gap, is a bit higher than the BCS value, corresponding to moderately coupled superconductivity in La_7Ni_3. These findings provide evidence that La_7Ni_3 might be a two-gap superconductor where both gaps open up at a common T_c and have a similar temperature dependence. Further experiments and theoretical band structure calculations are required to shed more light on the two-gap feature in La_7Ni_3.

B. Transverse-field μSR and penetration depth

To obtain complementary information on the nature of the superconducting gap, transverse-field (TF) μSR measurements were performed on La_7Ni_3. Magnetic fields in the range 10 mT to 40 mT, well above the lower critical field and perpendicular to the initial muon spin direction, were applied before cooling it through T_c to 0.1 K. This generates a well-ordered flux line lattice in the mixed superconducting state of a type II superconductor, resulting in a distinctive field distribution throughout the sample. The muon asymmetry spectra for temperatures above and below T_c are shown in Fig. 2. For $T > T_c$, spectra show a weak depolarization rate because of the nuclear dipolar fields and also confirm the homogeneous field distribution throughout the sample. In contrast, below T_c, the pronounced Gaussian damping attributes to the inhomogeneous field distribution in the flux line lattice. The time-domain spectra are best described by the sum of sinusoidally oscillating functions, each damped with a Gaussian relaxation component [57,58],

$$A(t) = \sum_{i=1}^{N} A_i \exp\left(-\frac{1}{2}\sigma_i^2 t^2\right) \cos(\gamma_\mu B_i t + \phi)$$
$$+ A_{bg} \cos(\gamma_\mu B_{bg} t + \phi), \tag{1}$$

where ϕ is the initial phase, A_i is the initial asymmetry, B_i is the mean field of the ith component of the Gaussian distribution, σ_i is the relaxation rate, and $\gamma_\mu/2\pi = 135.5$ MHz/T is the muon gyromagnetic ratio. A_{bg} and B_{bg} are the

temperature-independent background contribution for asymmetry and field, respectively, which originates from the muon stopping at the sample holder. Two Gaussian components ($N = 2$) are found sufficient to fit the time spectra for our sample. The second-moment method [59] is applied to calculate the temperature dependence of the total depolarization rate σ for different applied magnetic fields. The first and second moments of the local magnetic field distribution $p(B)$ for $N = 2$ are given by [59]:

$$\langle B \rangle = \sum_{i=1}^{2} \frac{A_i B_i}{A_1 + A_2}, \tag{2}$$

$$\langle \Delta B^2 \rangle = \frac{\sigma^2}{\gamma_\mu^2} = \sum_{i=1}^{2} \frac{A_i[(\sigma_i/\gamma_\mu)^2 + (B_i - \langle B \rangle)^2]}{A_1 + A_2},$$

where $\langle \cdot \rangle$ denotes average over magnetic fields. Figure 3(a) displays the resultant $\sigma(T)$. It has an almost constant value above T_c, which is due to the contribution of the nuclear dipo-
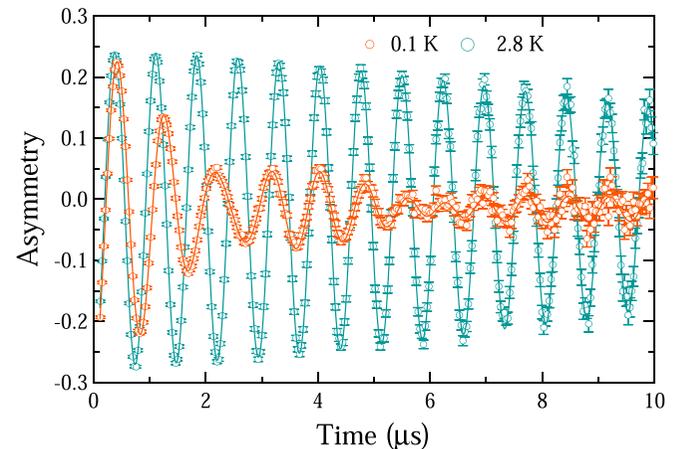
FIG. 2. The time-domain TF spectra taken above and below T_c in an applied magnetic field of 10 mT. The solid lines show the fitting using Eq. (1).
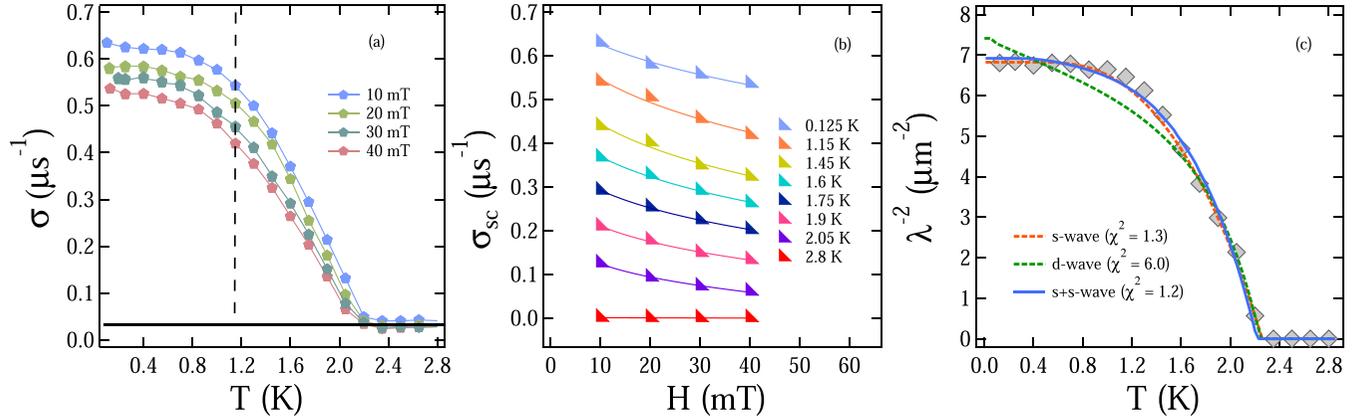
FIG. 3. (a) Temperature dependence of the muon spin depolarization rate at different applied magnetic fields from 10 mT to 40 mT in TF-μSR measurements. The approximately constant value in the normal state is indicated by the solid black line. (b) $\sigma_{sc}(H)$ at various temperatures ($T = 0.125$ K to $T = 2.80$ K), including the one designated by the dashed line in (a). The data were fitted using Eq. (3) to extract the temperature dependence of the inverse square of the magnetic penetration depth. (c) The calculated $\lambda^{-2}(T)$ where the solid line represents the best fit using Eq. (5).

lar field, $\sigma(T \gtrsim T_c) \simeq \sigma_{\text{ndip}} = 0.0333 \ \mu s^{-1}$ [represented by horizontal solid line in Fig. 3(a)]. The superconducting contribution σ_{sc} was extracted by subtracting $\sigma_{\text{ndip}} = 0.0333 \ \mu s^{-1}$ from σ using the following expression: $\sigma_{sc} = (\sigma^2 - \sigma_{\text{ndip}}^2)^{1/2}$. Figure 3(b) represents σ_{sc}, evaluated using isothermal cuts perpendicular to the temperature axis of the $\sigma(T)$ data sets in Fig. 3(a). The magnetic-field dependence of the penetration depth, λ_L, for Ginzburg-Landau parameters $\kappa_{GL} \geqslant 5$ (we estimate $\kappa_{GL} \simeq 26$, see Appendix A) is given by [60]

$$\sigma_{sc}(\mu s^{-1}) = 4.854 \times 10^4 (1-b)[1 + 1.21(1-\sqrt{b})^3]\lambda^{-2}, \tag{3}$$

for small reduced magnetic fields $b = \langle B \rangle / B_{c2}(T)$. Equation (3) was fitted to each σ_{sc} curve in order to extract the temperature dependence of λ. Figure 3(c) represents the behavior of the corresponding $\lambda^{-2}(T)$. To gain information about the form of the superconducting gap from $\lambda^{-2}(T)$, the latter can be expressed in the semiclassical approximation as [18,61,62]

$$\frac{\lambda^{-2}(T, \Delta_0)}{\lambda^{-2}(0, \Delta_0)} = 1 + \frac{1}{\pi} \int_0^{2\pi} \int_{\Delta(T,\phi)}^{\infty} \frac{\partial f}{\partial E} \frac{E dE d\phi}{\sqrt{E^2 - \Delta(T,\phi)^2}}, \tag{4}$$

where we have, for concreteness, focused on an isotropic 3D system with a gap $\Delta(T, \phi)$ that only depends on the azimuthal angle ϕ and $f = [\exp(E/k_B T) + 1]^{-1}$ is the Fermi-Dirac function. We use $\Delta(T, \phi) = \Delta_0 \delta(T/T_c) g(\phi)$, where $\delta(T/T_c) = \tanh[1.82(1.018((T_c/T) - 1))^{0.51}]$ describes (approximately) the temperature dependence of the overall gap magnitude, and $g(\phi)$ captures its angular dependence. We have $g(\phi) = 1$ for an isotropic gap function; note that such a gap function is not only consistent with s-wave pairing but also with the (single-gap limit of the) $E_2(1, i)$-wave and $s + is$ pairing states discussed below. For a d-wave state, it holds $g(\phi) = |\cos(2\phi)|$, leading to nodal points for $\phi = \pm \pi/4, \pm 3\pi/4$. To capture a possible two-gap scenario, we use a weighted sum [12]

$$\frac{\lambda^{-2}(T)}{\lambda^{-2}(0)} = x \frac{\lambda^{-2}(T, \Delta_{0,1})}{\lambda^{-2}(0, \Delta_{0,1})} + (1-x) \frac{\lambda^{-2}(T, \Delta_{0,2})}{\lambda^{-2}(0, \Delta_{0,2})}, \tag{5}$$

where $x \leqslant 0.5$ without loss of generality. Exactly as in the multigap α model for the specific heat above, the factor x in Eq. (5) expresses the fact that the density of states (or Sommerfeld coefficients) of the parts of the Fermi surface with gap $\Delta_{0,1}$ and $\Delta_{0,2}$ are in general different ($x \neq 0.5$).

The data shown in Fig. 3(c) was fitted with various models, consisting of a single isotropic gap [Eq. (4) with $g(\phi) = 1$], a single d-wave gap [$g(\phi) = |\cos(2\phi)|$ in Eq. (4)], and a model with two isotropic gaps [Eq. (5) with $g(\phi) = 1$]. As can be seen, a nodal d-wave scenario is not consistent with the data, in accordance with our discussion of the specific heat. While both single- and two-gap s-wave models yield good agreement, the fit is slightly better for the latter ($\chi^2 = 1.2$). More importantly, the best fit is obtained for a quite significant imbalance of the gap magnitudes, $\Delta_{0,2}(0)/\Delta_{0,1}(0) \simeq 2.7$, where the larger gap is hosted by the Fermi pocket(s) with the larger density of states—again, in line with the specific heat. The absolute values, however, of the gaps, $\Delta_{0,1}(0) = 0.18$ meV [$\Delta_{0,1}/k_B T_c = 0.94$] and $\Delta_{0,2}(0) = 0.49$ meV [$\Delta_{0,2}(0)/k_B T_c = 2.57$], are a bit larger and x is smaller than the corresponding values obtained from the specific heat. This discrepancy might be attributed to various approximations of our modeling, such as the assumption of isotropy and the fact that we neglected interband scattering. Notwithstanding this slight discrepancy, our specific heat and penetration depth measurements coherently indicate the presence of two fully established but significantly distinct superconducting gaps in La$_7$Ni$_3$.

C. Zero-field μSR and broken TRS

Zero-field muon spin relaxation (ZF-μSR) measurements were carried out to search for the presence of TRS breaking in La$_7$Ni$_3$. The ZF-μSR asymmetry spectra recorded below ($T = 0.2$ K) and above ($T = 2.9$ K) $T_c = 2.3$ K are shown in Fig. 4(a). The spectra do not exhibit any oscillatory components, which rules out the presence of any long-range magnetically ordered state. The asymmetry spectra recorded below and above T_c show an appreciable change in the
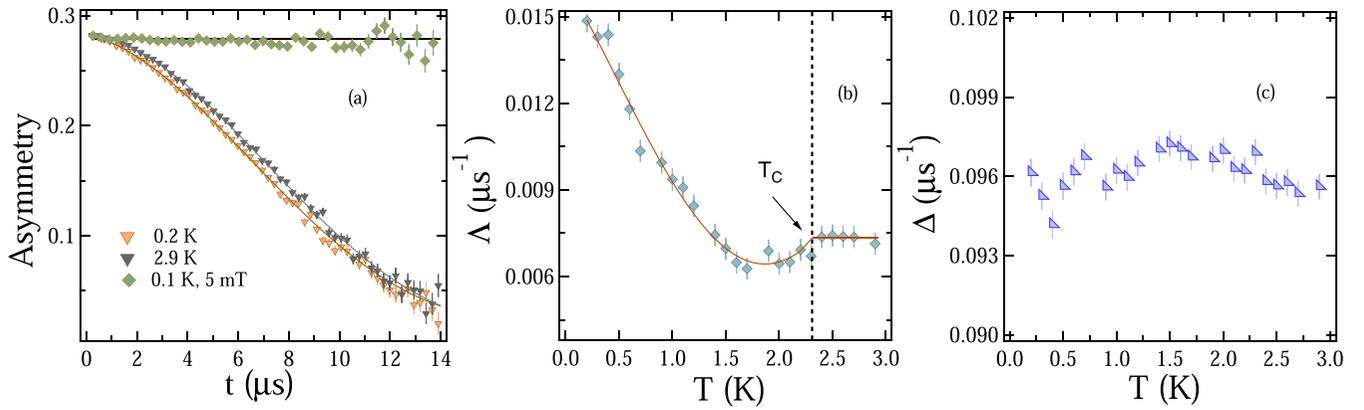
FIG. 4. (a) The asymmetry spectra collected at 0.2 K (orange) and 2.9 K (brown) in ZF-μSR, together with the LF-μSR data taken at 0.1 K in an applied field of 5 mT (green). The solid lines are fits of Eq. (7). (b) $\Lambda(T)$ exhibits a significant increase below $T_c = 2.3$ K and suggests the appearance of a spontaneous magnetic field in the superconducting state. (c) Temperature dependence of Δ, the relaxation of muon spins due to the static distribution of magnetic fields produced by nuclear magnetic moments which shows no dependence on temperature.

relaxation rates, and the stronger relaxation rate below T_c indicates the presence of internal magnetic field fluctuations in the superconducting state.

In the absence of atomic moments and at low temperatures where muon diffusion is not appreciable, the relaxation rate is expected to arise from the local fields associated with the nuclear moments. In this case, the behavior of asymmetry spectra is described by the Gaussian Kubo-Toyabe (KT) function [63]

$$G_{KT}(t) = \frac{1}{3} + \frac{2}{3}(1 - \Delta^2 t^2)\exp\left(\frac{-\Delta^2 t^2}{2}\right) \qquad (6)$$

where Δ represents the relaxation of muon spin due to the randomly oriented, static nuclear moments experienced at the muon site. The following function gives the best description of the ZF spectra for La_7Ni_3:

$$A(t) = A_0 G_{KT}(t)\exp(-\Lambda t) + A_1, \qquad (7)$$

where A_0 is the initial sample-related asymmetry, A_1 is the background contribution to the asymmetry from the muons stopping in the sample holder whereas Λ accounts for the electronic relaxation channels. The only parameter which exhibits a significant change as a function of temperature is the electronic relaxation rate Λ as shown in Fig. 4(b), while A_0, A_1, and Δ, see Fig. 4(c), are found to be temperature independent. The magnetic field of 5 mT was sufficient to decouple the muon spins from the relaxation channel, as shown in Fig. 4(a). This points towards the presence of a static or quasistatic magnetic field and excludes the possibility of any extrinsic effects such as magnetic impurities. Since for any ordered magnetic impurity, a significantly higher value of the longitudinal field would be required to decouple the muon spins from the impurity-induced relaxation channel. Such a notable increase in Λ below the onset of superconductivity suggests the appearance of a spontaneous magnetic field, providing convincing evidence of TRS breaking on entering the superconducting state of La_7Ni_3. Note that the signal corresponding to TRS breaking in La_7Ni_3 is similar to the one observed in other materials such as Sr_2RuO_4 [64], $LaNiC_2$ [40], $SrPtAs$ [41], $Lu_5Rh_6Sn_{18}$ [65], $Y_5Rh_6Sn_{18}$ [39], $Ba_{1-x}K_xFe_2As_2$ [66], $4Hb$-TaS_2 [67], and La_7Ir_3 [45] which

is considered to be a clear indication of broken TRS in these materials. Our data also imply a dilute distribution of the sources of the TRS-breaking field. The increase in the relaxation rate below T_c is 0.0081 μs^{-1} and the corresponding characteristic field strength is $\Lambda/\gamma_\mu = 0.1$ G. Similar strength is reported for other compounds with superconducting states that break TRS [40,41,45,50,65]. Moreover, the relaxation due to the randomly oriented, static nuclear dipolar fields from TF and ZF measurements represented by σ_{TF}^{dip} and Δ_{ZF}^{dip}, respectively, have a relation as follows: Δ_{ZF}^{dip} decays approximately $\sqrt{5}$ times faster than the σ_{TF}^{dip} [63]. Considering $\sigma_{TF}^{dip} = 0.0333$ μs^{-1} [as shown by horizontal solid line in Fig. 3(a)], and $\Delta_{ZF}^{dip} = 0.0963$ μs^{-1} [by taking the average of all temperature data points as shown in Fig. 4(c)], the ratio $\Delta_{ZF}^{dip}/\sigma_{TF}^{dip}$ is found out to be $1.29 \times \sqrt{5}$ for La_7Ni_3 which is pretty close to the expected ratio.

Following T_c, there is first a decrease in Λ upon lowering T below the normal state value and the true increase in Λ starts at $T_{onset} \simeq 1.7$ K. This leads to the small diplike feature in Fig. 4(b). We emphasize that there is no indication for any second phase transition from other measurements such as TF μSR (penetration depth) and specific heat. However, this type of feature with $T_{onset} < T_c$ has also been observed for other superconducting compounds such as in the odd-parity triplet state candidates $PrPt_4Ge_{12}$, $Pr_{1-x}Ce_xPt_4Ge_{12}$, $Pr_{1-x}La_xPt_4Ge_{12}$ [68–70], which are also believed to exhibit only a single superconducting transition. In these materials, screening of diluted magnetic impurity dipolar field was suggested as one of the origins [68], but a later work indicated that the mechanism is too weak to originate this effect [69]. The possibilities corresponding to the presence of impurities for La_7Ni_3 are discussed as follows: (i) Any small presence of dilute rare earth impurity (La < 0.03%) would lead to dynamic dipolar fields whose contribution can be seen from Lorentzian-Kubo Toyabe or root exponential term to muon relaxation. In any case, it will show a smooth variation with respect to temperature. (ii) The presence of residual ferromagnetic impurity (Ni < 1%) will result in reduced initial asymmetry. No such effects were noticed in our sample to discard the possibility of any such magnetic impurity. The

Voigtian function, which is a convolution of Lorentzian and Gaussian field distribution, has also been tried to fit the zero-field asymmetry spectra. Still, the obtained results were the same as for the static Kubo-Toyabe times exponential decay function with a diplike feature in Λ. Hence, at the moment, we do not have an explanation for the dip observed.

IV. DISCUSSION

We next discuss the implications of these experimental findings for the microscopic form and origin of the superconducting phase in La_7Ni_3. We describe two possible microscopic scenarios separately. Since mean-free path and coherence length are estimated to be of the same order of magnitude in our sample, we also comment on the impact of disorder for these two different scenarios.

A. A single transition and $E_2(1, i)$ pairing

Since there are currently no direct indications of two consecutive superconducting transitions, let us first assume that the TRS-breaking phase is reached by a single, continuous phase transition. Then the superconducting order parameter must transform under an irreducible representation (IR) of the point group, C_{6v}, of the crystal. Only multidimensional IRs, i.e., E_1 or E_2 for our case of C_{6v}, are consistent with broken TRS. As already discussed in Ref. [50], among the two associated superconductors $E_{1,2}(1, i)$ that break TRS, $E_1(1, i)$ is a less natural candidate: This follows from the observation that it generically gives rise to line nodes, signs of which are not seen in our data. $E_2(1, i)$, however, can be gapless as long as no nondegenerate Fermi surfaces go through the high-symmetry lines indicated in the inset of Fig. 5(a) and will, otherwise, exhibit point nodes.

To describe this pairing state microscopically, we first note that the broken inversion symmetry together with the presence of spin-orbit coupling removes the spin degeneracy of the bands. Therefore, spin is not a good quantum number at a generic crystal momentum $\boldsymbol{k}$ anymore and it is more natural [47] to study the projection, $\Delta(\boldsymbol{k}) \in \mathbb{C}$, of the superconducting order parameter (multiplied by the unitary part of the time-reversal operator) onto the band closest to or at the Fermi level at $\boldsymbol{k}$. For the $E_2(1, i)$ pairing state, it has the form $\Delta(\boldsymbol{k}) = \chi_1(\boldsymbol{k}) + i\,\chi_2(\boldsymbol{k})$, where χ_1 and χ_2 are real-valued and Brillouin-zone-periodic basis functions transforming as $k_x^2 - k_y^2$ and $2k_xk_y$ under C_{6v}; $\chi_{1,2}(\boldsymbol{k})$ are further required to be even under $\boldsymbol{k} \to -\boldsymbol{k}$ as a consequence of Fermi statistics and TRS [47]. Here $k_{x,y}$ are momenta in the *ab* plane of the system and perpendicular to two of the six mirror planes of C_{6v}. In Fig. 5(a), we show the resulting phase $\varphi_{\boldsymbol{k}}$ of the order parameter, $\Delta(\boldsymbol{k}) = e^{i\varphi_{\boldsymbol{k}}}|\Delta(\boldsymbol{k})|$, for the lowest-order (i.e., with fewest number of zeros) basis functions, $\chi_1(\boldsymbol{k}) = \cos(k_x/2)\cos(\sqrt{3}k_y/2) - \cos k_x$, $\chi_2(\boldsymbol{k}) = \sqrt{3}\sin(k_x/2)\sin(\sqrt{3}k_y/2)$, where we set $a = 1$. We see that $e^{i\varphi_{\boldsymbol{k}}}$ is a smooth function, except for the Γ-A and the $K^{(\prime)}$-$H^{(\prime)}$ lines, where both $\chi_{1,2}$ and, thus, the gap vanish due to threefold rotation symmetry C_3^z along z.

While we do not know the precise form of the Fermi surfaces of the system, we expect several pockets [71]. For illustration purposes, we show pockets (in gray) encircling
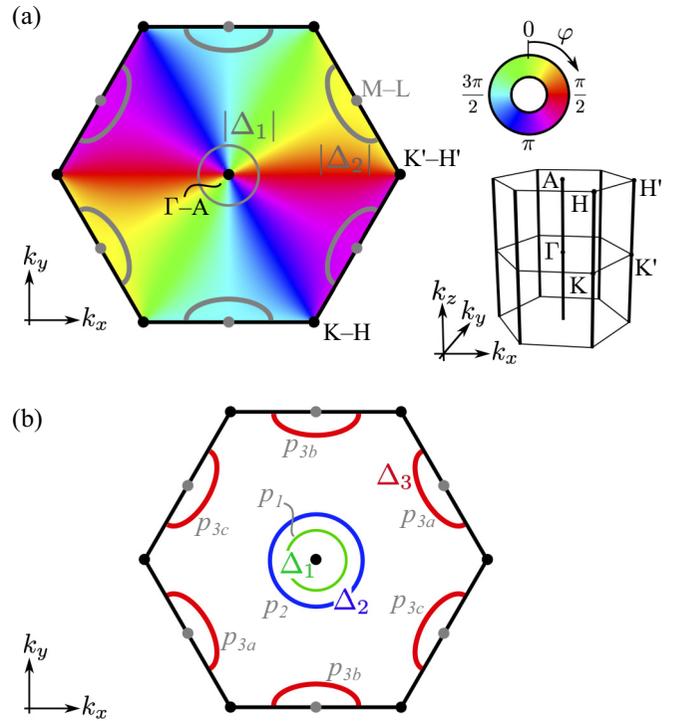
FIG. 5. Schematic illustration of the two possible pairing scenarios, $E_2(1, i)$ and $s + i s$, consistent with experiment. (a) Phase of the order parameter (color) for the $E_2(1, i)$ state in a 2D cut (at fixed k_z) of the Brillouin zone for the lowest-order basis functions. As long as no Fermi surfaces (such as the examples shown in gray) go through the high-symmetry lines marked by black dots (thick black lines in the inset), the state is fully gapped. As indicated by the thickness of the gray lines, the gap in generals differs on symmetry-unrelated Fermi pockets, $|\Delta_1| \neq |\Delta_2|$, in agreement with experiment. For the $s + i s$ state, shown in (b), the TRS breaking results from nontrivial relative phases (indicated by colors) of the order parameter between pockets that are not related by symmetry, i.e., $\Delta_j/|\Delta_j|$ depends on j.

both the Γ-A and the three M-L lines in Fig. 5(a). The gap, given by $|\Delta(\boldsymbol{k})|$, is constrained by symmetry to be the same (and here approximated to be constant, $|\Delta(\boldsymbol{k})| = \Delta_2$) on the three disconnected sheets at the boundary of the Brillouin zone, enclosing the three symmetry related M-L lines. It is generically not equal to that (Δ_1) in the Brillouin-zone center; $\Delta_1 \neq \Delta_2$ will give rise to the two-gap behavior seen in the specific heat and penetration depth. Note that, in this scenario, the $\boldsymbol{k}$-dependent phase that breaks TRS occurs between parts of the Fermi surface that are related by symmetry, such as the three pockets at the Brillouin-zone boundary which are related by C_6^z and exhibit a relative phase of (approximately) $e^{2\pi i/3}$.

Such a pairing state is expected to be realized, for instance, when the dominant interaction in the Cooper channel is a repulsion between the three pockets at the Brillouin-zone boundary in Fig. 5(a); we refer to the toy model in Appendix B for an illustration. In fact, it was very generally shown [48] that conventional electron-phonon pairing alone cannot give rise to a TRS-breaking superconducting state. Instead, an unconventional mechanism is required, associated with the fluctuation of a time-reversal-odd collective electronic mode, such as spin fluctuations.

B. Two consecutive transitions and $s + is$ pairing

A totally different route to TRS-breaking, full-gap superconductivity proceeds by two consecutive transitions, which could be too close to be resolved experimentally. Such a scenario arises when the dominant repulsive Cooper-channel interactions in the system scatter Cooper pairs of symmetry-*un*related parts of the Fermi surface—for instance between the three symmetry-unrelated sets of sheets p_1, p_2, and $p_3 = p_{3a} \cup p_{3b} \cup p_{3c}$ in Fig. 5(b). Let us assume that $\Delta_{\bm{k}}$ only varies weakly on each of the pockets and approximate $\Delta_{\bm{k}} = \Delta_j$ if $\bm{k} \in p_j$. The system is "frustrated" in the sense that these interactions favor $\Delta_1 = -\Delta_2$, $\Delta_1 = -\Delta_3$, but also $\Delta_2 = -\Delta_3$ simultaneously. If these dominant interactions are of the same order, the best compromise consists of nontrivial relative complex phases between $\Delta_{1,2,3}$, shown as differently colored Fermi pockets in Fig. 5(b). These relative phases break TRS and lead to spontaneous fields [72] that can be detected by our ZF-μSR measurements. Note that this fully-gapped $s + is$ state, with complex phases between symmetry-*un*related parts of the Fermi surface, cannot be reached by a single second-order phase transition as it transforms trivially under C_{6v} (IR A_1) and yet breaks TRS. Instead, there have to be two consecutive transitions and $\Delta(\bm{k}) = \eta_{s_1}(T)\chi_{s_1}(\bm{k}) + \eta_{s_2}(T)\chi_{s_2}(\bm{k})$, with $\chi_{s_j}(g\bm{k}) = \chi_{s_j}(\bm{k}) \in \mathbb{R}$ for all $g \in C_{6v}$ but changing sign between different p_j; at T_{c1}, first $\eta_{s_1} \neq 0$ while η_{s_2} only becomes finite below $T_{c2} < T_{c1}$, with a nontrivial complex phase relative to η_{s_1}. The two temperatures can get very close if the different dominant interaction scales (times the respective density of states) are close to each other. We further illustrate this in Appendix B and also point out that it is conceptually related to the mechanism of TRS breaking believed to be realized in certain (centrosymmetric) iron-based superconductors [66,73].

C. Relevance of disorder

Finally, our measurements indicate (see Appendix A) that the electronic mean-free path l of our sample of La$_7$Ni$_3$ is of the same order as the superconducting coherence length ξ. One would, thus, naively expect that any superconducting state with a significantly momentum-dependent order parameter, such as the $\bm{k}$-dependent phases of $\Delta(\bm{k})$ above, should be strongly suppressed [74,75]. However, more recent theoretical works [20–24] have shown that the pair-breaking effect of impurities can be significantly reduced in the presence of spin-orbit coupling; this is also confirmed by experiments [25–27] indicating that the critical temperature of pairing states transforming under a nontrivial representation of the point group might only be weakly suppressed in the presence of spin-orbit coupling—even when l becomes smaller than ξ (or even of the order of the Fermi wavelength). The basic reason for this protection mechanism is that matrix elements of an impurity potential between certain pairs $(\bm{k}_1, \bm{k}_2)$ of momenta can be suppressed due to spin-orbit mixing and that only certain scattering processes are pair breaking. As follows immediately from the generalized Anderson theorem of Refs. [23,76,77] (see Appendix B for more details), the $E_1(1, i)$ state in Fig. 5(a), for instance, is not affected by scattering within each of the three pockets at the zone boundaries. Similarly, the $s + is$ state is protected against scattering

events where both $\bm{k}_1$ and $\bm{k}_2$ belong to one of the three sets of sheets p_1, p_2, and p_3. We, thus, believe that systematic combined experimental and theoretical studies of the impact of disorder can provide further information about the form of the superconducting pairing state.

V. SUMMARY AND CONCLUSION

In summary, we have studied the superconducting state of La$_7$Ni$_3$, the most recent member of the Th$_7$Fe$_3$ family of superconductors, using a combination of specific heat, TF-μSR, and ZF-μSR measurements. Both specific heat and TF measurements reveal the presence of two significantly distinct superconducting gaps, which are both found to be nodeless and isotropic. In ZF measurements, we have detected a static internal magnetic field that starts to develop below the superconducting transition temperature and grows as we further decrease temperature; this provides substantial evidence for TRS breaking and, hence, reveals the unconventional nature and pairing mechanism [48] of the superconducting state of La$_7$Ni$_3$. The change in the relaxation rate for La$_7$Ni$_3$ is almost equivalent to other compounds such as La$_7$Ir$_3$ and La$_7$Rh$_3$. This points towards the relevance of La in inducing the unconventional superconducting state in this family of materials. We have discussed possible microscopic scenarios for the order parameter and pairing interactions of the superconducting phase. In order to pinpoint which of those possibilities is realized, further experimental work on single crystals of La$_7$Ni$_3$, in particular, uniaxial and hydrostatic pressure studies [78], theoretical modeling, and band structure calculations are required.

APPENDIX A: PARAMETERS OF La$_7$Ni$_3$ FROM DATA

1. Critical fields

To determine the lower critical field, $H_{c1}(T = 0)$, field-dependent magnetization, $M(H)$, measurements have been performed with T ranging from 1.8 K to 2.16 K, as shown in the inset of Fig. 6(a). H_{c1} is defined as the value of H where $M(H)$ starts to deviate from linearity. The main panel of Fig. 6(a) shows the estimated value of H_{c1} as a function of T. The solid blue line is a fit to the data using the following equation:

$$H_{c1}(T) = H_{c1}(0)\left[1 - \left(\frac{T}{T_c}\right)^2\right]. \quad (A1)$$

It provides $H_{c1}(0) = 5.19 \pm 0.07$ mT.

The upper critical field has been extracted from the $\chi(T)$ curves in the inset of Fig. 6(b), measured at different magnetic
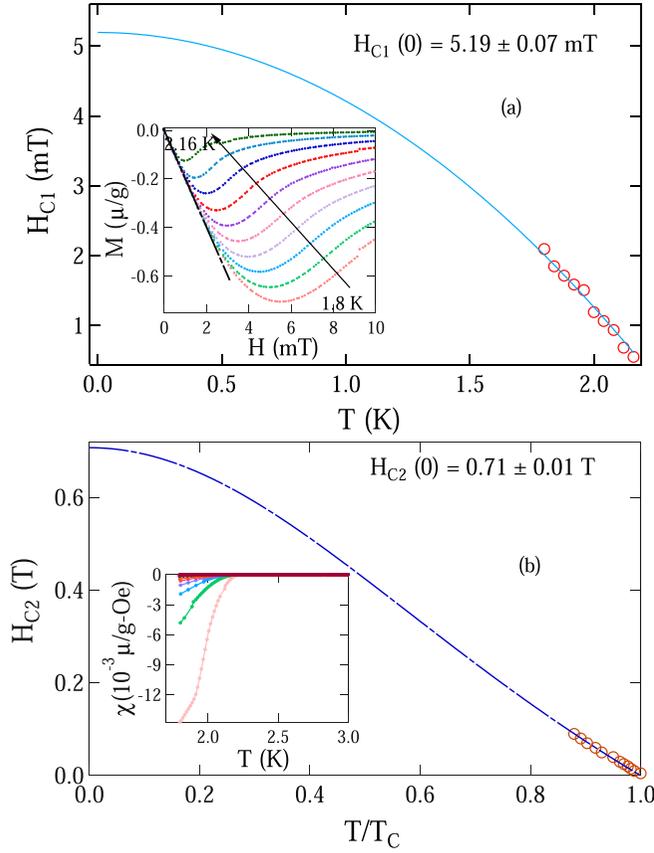
FIG. 6. (a) Lower critical field H_{c1} as a function of temperature. Inset shows the low-field magnetization curves obtained at different fixed temperatures. (b) Upper critical field H_{c2} of La$_7$Ni$_3$ versus temperature, where the blue line represents a fit with Eq. (A2). Inset shows the susceptibility as a function of temperature at different fields.

fields starting from 5 mT to 90 mT by considering the onset of the diamagnetic signal. Figure 6(b) shows a linear behavior in $H_{c2}(T)$ when plotted with respect to temperature and can be well described using the Ginzburg-Landau equation

$$H_{c2}(T) = H_{c2}(0)\frac{1 - t^2}{1 + t^2}, \qquad \text{(A2)}$$

where $t = T/T_c$. The data fits well and provides $H_{c2}(0) = 0.71 \pm 0.01$ T. The Pauli paramagnetic limit is given by $H_{c2}^P(0) = C\,T_c$, where $C = 1.86\,T/K$. It is evaluated to be 4.28 T which is higher than the value of the upper critical field and indicates the dominance of spin singlet component in the superconducting state.

The value of $H_{c2}(0)$ is also used to determine the Ginzburg-Landau coherence length $\xi_{GL}(0)$ by using the expression [79]: $H_{c2}(0) = \frac{\Phi_0}{2\pi \xi_{GL}^2}$ where Φ_0 $(= 2.07 \times 10^{-15}$ Tm^2) is the superconducting magnetic-flux quantum. For $H_{c2}(0) = 0.71\,T$, $\xi_{GL}(0)$ is evaluated to be 215 Å. In order to calculate the Ginzburg-Landau penetration depth $\lambda_{GL}(0)$, the values of $\xi_{GL}(0)$ and $H_{c1}(0)$ can be employed in the relation [79]:

$$H_{c1}(0) = \frac{\Phi_0}{4\pi \lambda_{GL}^2(0)}\left(\ln\frac{\lambda_{GL}(0)}{\xi_{GL}(0)} + 0.12\right). \qquad \text{(A3)}$$
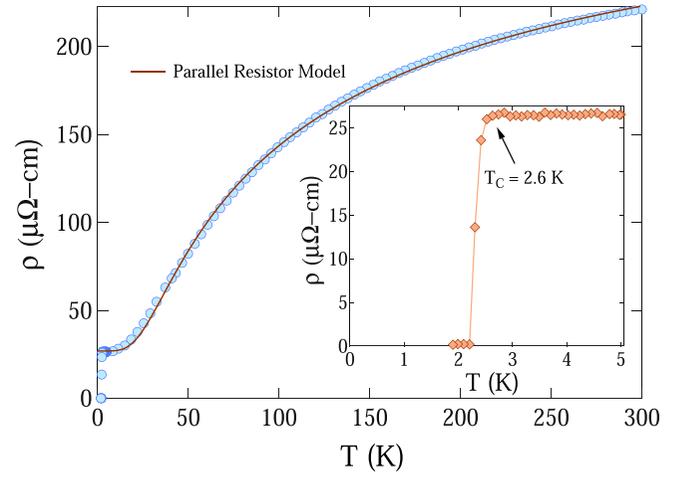
FIG. 7. Resistivity as a function of temperature in zero applied field over the range 1.9 K $\leqslant$ T $\leqslant$ 300 K. The line shows a fitting with parallel resistor model. Inset: $\rho(T)$ at low temperature exhibiting a drop in resistivity at $T_{c,\text{onset}} = 2.6$ K.

With $H_{c1}(0) = 5.19$ mT and $\xi_{GL}(0) = 215$ Å, we find $\lambda_{GL}(0) = 2940$ Å. Consequently, the Ginzburg-Landau parameter $\kappa_{GL} = \frac{\lambda_{GL}(0)}{\xi_{GL}(0)} = 26$ suggests that La$_7$Ni$_3$ is a strong type II superconductor. All the calculated parameters are summarized in Table I together with its isostructural compounds La$_7$Rh$_3$ and La$_7$Ir$_3$. We finally note that the expressions we use to extract these parameters are not generally guaranteed to be accurate, in particular in the vicinity of the transition [80], in the case of the $s + is$ scenario, which involves two consecutive transitions.

2. Electrical resistivity

Electrical resistivity measurements in the temperature range 1.9 K to 300 K have been performed in zero applied field and are shown in Fig. 7. Inset shows the zero-resistivity drop with onset temperature $T_{c,\text{onset}} = 2.6$ K. Above $T \simeq 50$ K, the resistivity data exhibits a saturationlike behavior which can occur when the mean free path is of the order of the interatomic spacing [81]. This type of behavior in $\rho(T)$ was described by Wiesmann *et al.* [82] by the following expression

$$\rho(T) = \left[\frac{1}{\rho_s} + \frac{1}{\rho_i(T)}\right]^{-1}, \qquad \text{(A4)}$$

where ρ_s is the temperature-independent saturation resistivity attained at higher temperatures and $\rho_i(T)$ is given by [83]

$$\rho_i(T) = \rho_{i,0} + C\left(\frac{T}{\Theta_D}\right)^5 \int_0^{\Theta_D/T} \frac{x^5}{(e^x - 1)(1 - e^{-x})}dx, \qquad \text{(A5)}$$

where $\rho_{i,0}$ represents the temperature-independent residual resistivity due to scattering from defects in the crystal structure; the second term in Eq. (A5) is a temperature-dependent contribution which can be described by the generalized BG model in which C is a material-dependent factor and Θ_D is the Debye temperature obtained from resistivity measurements. The red dashed line in the main panel of Fig. 7 shows the best fitting to

the data and yields $\rho_0 = 29.6 \pm 0.3 \; \mu\Omega$ cm, $C = 1674 \pm 39$ $\mu\Omega$ cm, $\rho_{0,s} = 303 \pm 1 \; \mu\Omega$ cm, and $\Theta_D = 152 \pm 2$ K.

3. Electronic properties

The Sommerfeld coefficient γ_n and quasiparticle number density n are related by

$$\gamma_n = \left(\frac{\pi}{3}\right)^{2/3} \frac{k_B^2 m^* V_{\text{f.u.}} n^{1/3}}{\hbar^2 N_A}, \tag{A6}$$

where k_B is the Boltzmann constant, $V_{\text{f.u.}}$ is the volume of a formula unit, N_A is the Avogadro number, and m^* is the effective mass of quasiparticles. The residual resistivity ρ_0 is related to Fermi velocity v_F and electronic mean free path l by the expression

$$l = \frac{3\pi^2 \hbar^3}{e^2 \rho_0 m^{*2} v_F^2}, \tag{A7}$$

whereas the Fermi velocity v_F can be expressed in terms of quasiparticle carrier density and effective mass by

$$n = \frac{1}{3\pi^2} \left(\frac{m^* v_F}{\hbar}\right)^3. \tag{A8}$$

The expression for the penetration depth $\lambda_{\text{GL}}(0)$ in the dirty limit is given by [79]

$$\lambda_{\text{GL}}(0) = \left(\frac{m^*}{\mu_0 n e^2}\right)^{1/2} \left(1 + \frac{\xi_0}{l}\right)^{1/2}, \tag{A9}$$

where ξ_0 is the BCS coherence length and the first term in the bracket represents the London penetration depth λ_L. In the dirty limit at $T = 0$ K, Ginzburg-Landau coherence length $\xi_{\text{GL}}(0)$ and BCS coherence length ξ_0 are related by the expression

$$\frac{\xi_{\text{GL}}(0)}{\xi_0} = \frac{\pi}{2\sqrt{3}} \left(1 + \frac{\xi_0}{l}\right)^{-1/2}. \tag{A10}$$

By providing the values of $\gamma_n = 44.44$ mJ mol^{-1} K^{-2}, $\xi_{\text{GL}}(0) = 215$ Å, and $\rho_0 = 29.6 \; \mu\Omega$-cm, the above equations were solved simultaneously which provides m$^* = 6.3$ m$_e$, $n = 4.3 \times 10^{27}$ m^{-3}, $l_e = 182$ Å, $\xi_0 = 202$ Å. The ratio of $\xi_0/l_e = 1.1$ indicates that the superconductor is characterized by significant disorder ("dirty limit"), which is consistent with published data [54].

APPENDIX B: TOY MODELS FOR TRS BREAKING

In this Appendix, we will discuss symmetry-based, phenomenological models for each of the two possible TRS-breaking pairing scenarios—the $E_2(1, i)$ and $s + is$ states—discussed in the main text. We will also briefly study their disorder sensitivity, using the results of Refs. [23,76].

1. $E_2(1, i)$ pairing model

To provide an example of how an $E_2(1, i)$ state can arise, let us assume that the energetics of superconductivity is mainly determined by the interactions between the three distinct pockets encircling the M-L lines in Fig. 5(a) and that the superconducting order parameter can be taken to be constant on each of these three separate sheets, $j = 1, 2, 3$,

with value $\Delta(\boldsymbol{k}) = \Delta_j$. Neglecting the subleading energetic contributions from other Fermi surfaces for simplicity, the superconducting free energy can be written as

$$\Delta\mathcal{F}(T) = \sum_{j,j'=1}^3 \Delta_j^* a_{jj'}(T) \Delta_{j'} + \ldots, \tag{B1}$$

where the ellipsis stands for terms higher order in the superconducting order parameter. It is straightforward to derive the representations of the symmetries on the superconducting order parameter: under time reversal, $\Delta_j \to \Delta_j^*$; under C_6^z, $\Delta_j \to \Delta_{j+1}$ (with $\Delta_4 \equiv \Delta_1$), and under σ_v, $\boldsymbol{\Delta} := (\Delta_1, \Delta_2, \Delta_3) \to (\Delta_3, \Delta_2, \Delta_1)$. Combined with $\Delta\mathcal{F} \in \mathbb{R}$, we thus end up with

$$a_{jj'}(T) = \alpha(T)\delta_{j,j'} + \beta(T)(1 - \delta_{j,j'}), \quad \alpha, \beta \in \mathbb{R}, \tag{B2}$$

such that the dominant superconducting instability [eigenvector of $a(T)$ with eigenvalue that first becomes negative upon lowering T to T_c] just depends on the sign of $\beta(T_c)$: If it is negative, which corresponds to *attractive interpocket interactions*, we get the *s*-wave state (transforming under IR A_1 of C_{6v})

$$\boldsymbol{\Delta} = \Delta_0(T)(1, 1, 1), \qquad \Delta_0(T) \in \mathbb{C}, \tag{B3}$$

which preserves TRS. For *repulsive interpocket interactions*, $\beta(T_c) > 0$, the leading instability is doubly degenerate,

$$\boldsymbol{\Delta} = \sum_{\mu=1,2} \eta_\mu \boldsymbol{\chi}_\mu, \quad \eta_\mu \in \mathbb{C},$$

$$\boldsymbol{\chi}_1 = \left(\frac{1}{\sqrt{6}}, -\sqrt{\frac{2}{3}}, \frac{1}{\sqrt{6}}\right), \quad \boldsymbol{\chi}_2 = \left(\frac{1}{\sqrt{2}}, 0, -\frac{1}{\sqrt{2}}\right),$$

with the two components $\boldsymbol{\chi}_{1,2}$ transforming as $k_x^2 - k_y^2$ and $2k_x k_y$ under C_{6v} and, hence, under the IR E_2. While the two complex numbers $\eta_{1,2}$ are determined by the higher-order terms omitted in Eq. (B1), it has been shown [47] that, irrespective of microscopic details, only the solution with a nontrivial relative complex phase, $\eta_2 = \pm i\eta_1$, is possible energetically for spin-orbit coupled noncentrosymmetric systems. Therefore, we end up with

$$\boldsymbol{\Delta} = \Delta_0(T)(1, \omega, \omega^2), \qquad \omega = e^{\frac{2\pi i}{3}}, \tag{B4}$$

in accordance with the form of the complex phase shown in Fig. 5(a).

To demonstrate the statements of the main text about which scattering processes are pair breaking, we employ the generalized form of the Anderson theorem of Ref. [76] (see Sec. 7.1 therein): For our case of singly-degenerate Fermi surfaces, a superconductor is protected against nonmagnetic, $t_W = +1$, (magnetic, $t_W = -1$) impurity scattering with matrix elements $W_{\boldsymbol{k},\boldsymbol{k}'}$ if the commutator (anticommutator)

$$C_{\boldsymbol{k},\boldsymbol{k}'} = \Delta(\boldsymbol{k}) W_{\boldsymbol{k},\boldsymbol{k}'} - t_W W_{\boldsymbol{k},\boldsymbol{k}'} \Delta(\boldsymbol{k}') \tag{B5}$$

vanishes. In fact, it was shown [23] that the same commutator also quantitatively determines how fragile a superconductor is, since the reduction $\delta T_c = T_c - T_{c,0}$ of the transition temperature T_c relative to its value in the clean limit $T_{c,0}$ can be written as

$$\delta T_c \sim -\frac{\pi}{4} \tau^{-1} \zeta \tag{B6}$$

for small total scattering rates $\tau^{-1} \to 0$. The sensitivity parameter reads as [23]

$$\zeta = \frac{||C||_{\rm F}^2}{4||W||_{\rm F}^2 \langle |\Delta|^2 \rangle_{\rm FS}}, \quad \text{(B7)}$$

where $||C||_{\rm F}^2 = \sum_{\bm{k},\bm{k}'}^{\rm FS} |C_{\bm{k},\bm{k}'}|^2$ is Frobenius norm on the Fermi surface (FS) and $\langle \cdot \rangle_{\rm FS}$ is the Fermi surface average (normalized such that $\langle 1 \rangle_{\rm FS} = 1$).

This expression is readily applied to any superconducting system and impurity potential [23,85]. For our model here, with order parameter given in Eq. (B4), the scattering matrix W effectively becomes a Hermitian 3×3 matrix, $W_{jj'} = W_{jj'}^*$, $j, j' = 1, 2, 3$. After straightforward matrix algebra, Eq. (B7) yields for nonmagnetic disorder ($t_W = +1$)

$$\zeta_{E_2(1,i)} = \frac{3\tau_{\rm inter}^{-1}}{4(\tau_{\rm intra}^{-1} + \tau_{\rm inter}^{-1})}, \quad \text{(B8)}$$

with inter- and intrasheet scattering rates given by $\tau_{\rm inter}^{-1} = 2(|W_{12}|^2 + |W_{13}|^2 + |W_{23}|^2)$ and $\tau_{\rm intra}^{-1} = \sum_{j=1}^3 |W_{jj}|^2$, respectively. In particular, it follows that only intersheet scattering is pair breaking, as stated in the main text. This can also be directly seen from the commutator (B5) of the generalized Anderson theorem, which vanishes for momentum pairs $(\bm{k}, \bm{k}')$ with $\Delta_{\bm{k}} = \Delta_{\bm{k}'}$ in the current case of nonmagnetic scattering ($t_W = 1$). Further note we get $\zeta = 1/2$ from Eq. (B8) for momentum-independent scattering matrix elements, $|W_{ij}| = $ const., as expected for a pairing state transforming under a nontrivial IR.

2. $s + i\,s$ pairing model

To illustrate how an $s + i\,s$ state can arise, let us consider three different sets of symmetry-unrelated Fermi pockets, such as p_1, p_2, and $p_3 = p_{3a} \cup p_{3b} \cup p_{3c}$ in Fig. 5(b). Since we are interested in s-wave pairing, we will assume that $\Delta(\bm{k})$ is invariant under all $g \in C_{6v}$ and, for simplicity, take it to be constant on each of these three sets of sheets, $\Delta(\bm{k}) = \Delta_j$ if $\bm{k} \in p_j$. The free energy can again be written in the form (B1) to quadratic order in Δ; however, since the pockets are not related by symmetry operators, there are fewer constraints on $a(T)$: It only needs to be real and symmetric, $a^T = a \in \mathbb{R}^{3 \times 3}$, due to $\Delta\mathcal{F} \in \mathbb{R}$ and TRS. Further assuming that the form of the pairing state is predominantly determined by the repulsion between the different pockets, we can use

$$a(T) \simeq \alpha_0(T) \mathbb{1}_{3\times 3} + \beta(T) \begin{pmatrix} 0 & 1 & 1+\delta_1 \\ 1 & 0 & 1+\delta_2 \\ 1+\delta_1 & 1+\delta_2 & 0 \end{pmatrix},$$

with $\beta(T) < 0$, $\delta_j > -1$. As such, the form of the leading instability only depends on the two real parameters $\delta_{1,2}$, which we rewrite according to $(\delta_1, \delta_2) = \delta(\cos\theta, \sin\theta)$. For $|\delta| \ll 1$,

two superconducting states are asymptotically degenerate and

$$\bm{\Delta} = (\Delta_1, \Delta_2, \Delta_3)^T = \sum_{\mu=\pm} \eta_\mu(T) \bm{\chi}_\mu, \quad \eta_\mu \in \mathbb{C}, \quad \text{(B9)}$$

where

$$\bm{\chi}_\pm \sim \mathcal{N}_\pm(\theta) \begin{pmatrix} \cos\theta - \sin\theta \pm \sqrt{1 - \cos\theta \sin\theta} \\ \sin\theta \\ \mp\sqrt{1 - \cos\theta \sin\theta} - \cos\theta \end{pmatrix}, \quad \text{(B10)}$$

with normalization factor $\mathcal{N}_\pm(\theta)$. As follows from the respective eigenvalues, η_+ (η_-) first becomes nonzero at T_{c1} upon cooling down while $\eta_- = 0$ ($\eta_+ = 0$), if $\delta > 0$ ($\delta < 0$). This first superconducting phase respects TRS since $\bm{\Delta}^* \propto \bm{\Delta}$. However, due to the near degeneracy of the states, a second transition can take place at which $\eta_- \neq 0$ ($\eta_+ \neq 0$), with transition temperature T_{c2}; note that $T_{c1} - T_{c2}$ becomes vanishingly small as $\delta \to 0$.

To obtain the relative weight and phase of η_+ and η_-, we need to go beyond quadratic order in $\Delta\mathcal{F}$. Among the quartic contributions to the free energy,

$$\gamma(T)\mathrm{Re}\left[(\eta_+^*)^2 \eta_-^2\right] \quad \text{(B11)}$$

is sensitive to the relative phase. It straightforwardly follows from the structure of the underlying one-loop diagram that $\gamma(T) > 0$, see, e.g., Ref. [73] for an explicit computation. Therefore, we obtain that the relative complex phase of η_+ and η_- is $\pi/2$ below T_{c2}. Since $\bm{\chi}_\pm$ in Eq. (B10) are linearly independent, the superconducting state breaks TRS as stated in the main text.

As follows from this discussion, the $s + i\,s$ state is possible as long as neither $\bm{\Delta} = \bm{\chi}_+$ nor $\bm{\Delta} = \bm{\chi}_-$ are suppressed by disorder. While it is straightforward to evaluate Eq. (B7) for the general form in Eq. (B10), let us for notational simplicity focus on $\delta_1 = \delta_2 \equiv \delta$ where $\bm{\chi}_+ \sim (1 + \delta/3, 1 + \delta/3, -2)^T$, to linear order in δ, and $\bm{\chi}_- \propto (-1, 1, 0)^T$. For $\bm{\chi}_-$, we then get

$$\zeta_- = \frac{3(\tau_{\rm inter}^{-1}/2 + 3|W_{12}|^2)}{4(\tau_{\rm intra}^{-1} + \tau_{\rm inter}^{-1})}, \quad \text{(B12)}$$

and $\bm{\chi}_+$ leads to

$$\zeta_+ = \frac{(9 + \delta)^2}{27 + \delta(6 + \delta)} \frac{3(|W_{13}|^2 + |W_{23}|^2)}{4(\tau_{\rm intra}^{-1} + \tau_{\rm inter}^{-1})}, \quad \text{(B13)}$$

where we again took $t_W = +1$. As expected, we see that, while $\bm{\chi}_-$ is particularly sensitive to scattering between the pockets p_1 and p_2, only scattering events between patches p_1 and p_3 and between p_2 and p_3 are pair breaking for $\bm{\chi}_+$, which can also be immediately inferred from the commutator (B5) directly. It is thus manifest that intrasheet scattering is not expected to suppress the $s + i\,s$ state.

[1] P. Anderson, Higgs, Anderson and all that, Nat. Phys. **11**, 93 (2015).

[2] T. H. Hansson, V. Oganesyan, and S. L. Sondhi, Ann. Phys. **313**, 497 (2004).

[3] M. Sigrist and K. Ueda, Rev. Mod. Phys. **63**, 239 (1991).

[4] E. Bauer and M. Sigrist, *Non-centrosymmetric Superconductor: Introduction and Overview* (Springer-Verlag, Heidelberg, 2012).

[5] E. I. Rashba, Sov. Phys. Solid State **2**, 1224 (1960).

[6] G. Dresselhaus, Phys. Rev. **100**, 580 (1955).

[7] L. P. Gor'kov and E. I. Rashba, Phys. Rev. Lett. **87**, 037004 (2001).

[8] E. Bauer, G. Hilscher, H. Michor, Ch. Paul, E. W. Scheidt, A. Gribanov, Yu. Seropegin, H. Noël, M. Sigrist, and P. Rogl, Phys. Rev. Lett. **92**, 027003 (2004).

[9] P. A. Frigeri, D. F. Agterberg, A. Koga, and M. Sigrist, Phys. Rev. Lett. **93**, 099903(E) (2004).

[10] T. Shang, G. M. Pang, C. Baines, W. B. Jiang, W. Xie, A. Wang, M. Medarde, E. Pomjakushina, M. Shi, J. Mesot, H. Q. Yuan, and T. Shiroka, Phys. Rev. B **97**, 020502(R) (2018).

[11] E. M. Carnicom, W. W. Xie, T. Klimczuk, J. J. Lin, K. Gornicka, Z. Sobczak, N. P. Ong, and R. J. Cava, Sci. Adv. **4**, eaar7969 (2018).

[12] D. A. Mayoh, A. D. Hillier, K. Götze, D. McK. Paul, G. Balakrishnan, and M. R. Lees, Phys. Rev. B **98**, 014502 (2018).

[13] J.-K. Bao, J.-Y. Liu, C.-W. Ma, Z.-H. Meng, Z.-T. Tang, Y.-L. Sun, and H.-F. Zhai, H. Jiang, H. Bai, C.-M. Feng, Z.-A. Xu, and G.-H. Cao, Phys. Rev. X **5**, 011013 (2015).

[14] H. Q. Yuan, D. F. Agterberg, N. Hayashi, P. Badica, D. Vandervelde, K. Togano, M. Sigrist, and M. B. Salamon, Phys. Rev. Lett. **97**, 017006 (2006).

[15] M. Nishiyama, Y. Inada, and G.-q. Zheng, Phys. Rev. Lett. **98**, 047002 (2007).

[16] A. Bhattacharyya, D. T. Adroja, K. Panda, Surabhi Saha, Tanmoy Das, A. J. S. Machado, O. V. Cigarroa, T. W. Grant, Z. Fisk, A. D. Hillier, and P. Manfrinetti, Phys. Rev. Lett. **122**, 147001 (2019).

[17] G. M. Pang, M. Smidman, W. B. Jiang, J. K. Bao, Z. F. Weng, Y. F. Wang, L. Jiao, J. L. Zhang, G. H. Cao, and H. Q. Yuan, Phys. Rev. B **91**, 220502(R) (2015).

[18] D. T. Adroja, A. Bhattacharyya, M. Telling, Yu. Feng, M. Smidman, B. Pan, J. Zhao, A. D. Hillier, F. L. Pratt, and A. M. Strydom, Phys. Rev. B **92**, 134505 (2015).

[19] P. K. Biswas, A. Iyo, Y. Yoshida, H. Eisaki, K. Kawashima, and A. D. Hillier, Phys. Rev. B **95**, 140505(R) (2017).

[20] K. Michaeli and L. Fu, Phys. Rev. Lett. **109**, 187003 (2012).

[21] M. S. Scheurer, M. Hoyer, and J. Schmalian, Phys. Rev. B **92**, 014518 (2015).

[22] D. C. Cavanagh and P. M. R. Brydon, Phys. Rev. B **101**, 054509 (2020).

[23] E. I. Timmons, S. Teknowijoyo, M. Konczykowski, O. Cavani, M. A. Tanatar, S. Ghimire, K. Cho, Y. Lee, L. Ke, N. H. Jo, S. L. Bud'ko, P. C. Canfield, P. P. Orth, M. S. Scheurer, and R. Prozorov, Phys. Rev. Res. **2**, 023140 (2020).

[24] D. Dentelski, V. Kozii, and J. Ruhman, Phys. Rev. Res. **2**, 033302 (2020).

[25] M. Kriener, K. Segawa, S. Sasaki, and Y. Ando, Phys. Rev. B **86**, 180505(R) (2012).

[26] Superconductor derived from a topological insulator heterostructure, S. Sasaki, K. Segawa, and Y. Ando, Phys. Rev. B **90**, 220504(R) (2014).

[27] M. P. Smylie, K. Willa, H. Claus, A. Snezhko, I. Martin, W.-K. Kwok, Y. Qiu, Y. S. Hor, E. Bokari, P. Niraula, A. Kayani, V. Mishra, and U. Welp, Phys. Rev. B **96**, 115145 (2017).

[28] J. Alicea, Rep. Prog. Phys. **75**, 076501 (2012).

[29] A. P. Schnyder and S. Ryu, Phys. Rev. B **84**, 060504(R) (2011).

[30] M. N. Ali, Q. D. Gibson, T. Klimczuk, and R. J. Cava, Phys. Rev. B **89**, 020505(R) (2014).

[31] Z. X. Sun, M. Enayat, A. Maldonado, C. Lithgow, E. Yelland, D. C. Peets, A. Yaresko, A. P. Schnyder, and P. Wahl, Nat. Commun. **6**, 6633 (2015).

[32] M. S. Scheurer and J. Schmalian, Nat. Commun. **6**, 6005 (2015).

[33] H. Kim, K. Wang, Y. Nakajima, R. Hu, S. Ziemak, P. Syers, L. Wang, H. Hodovanets, J. D. Denlinger, P. M. R. Brydon, D. F. Agterberg, M. A. Tanatar, R. Prozorov, and J. Paglione, Sci. Adv. **4**, eaao4513 (2018).

[34] P. W. Anderson, J. Phys. Chem. Solids **11**, 26 (1959).

[35] M. Smidman, A. D. Hillier, D. T. Adroja, M. R. Lees, V. K. Anand, R. P. Singh, R. I. Smith, D. McK. Paul, and G. Balakrishnan, Phys. Rev. B **89**, 094509 (2014).

[36] S. K. P., D. Singh, P. K. Biswas, A. D. Hillier, and R. P. Singh, Phys. Rev. B **98**, 214505 (2018).

[37] T. Shang, W. Wei, C. Baines, J. L. Zhang, H. F. Du, M. Medarde, M. Shi, J. Mesot, and T. Shiroka, Phys. Rev. B **98**, 180504(R) (2018).

[38] T. Shang, J. Philippe, J. A. T. Verezhak, Z. Guguchia, J. Z. Zhao, L. J. Chang, M. K. Lee, D. J. Gawryluk, E. Pomjakushina, M. Shi, M. Medarde, H. R. Ott, and T. Shiroka, Phys. Rev. B **99**, 184513 (2019).

[39] A. Bhattacharyya, D. T. Adroja, N. Kase, A. D. Hillier, J. Akimitsu, and A. M. Strydom, Sci. Rep. **5**, 12926 (2015).

[40] A. D. Hillier, J. Quintanilla, and R. Cywinski, Phys. Rev. Lett. **102**, 117007 (2009).

[41] P. K. Biswas, H. Luetkens, T. Neupert, T. Stürzer, C. Baines, G. Pascua, A. P. Schnyder, M. H. Fischer, J. Goryo, M. R. Lees, H. Maeter, F. Brückner, H.-H. Klauss, M. Nicklas, P. J. Baker, A. D. Hillier, M. Sigrist, A. Amato, and D. Johrendt, Phys. Rev. B **87**, 180503(R) (2013).

[42] R. P. Singh, A. D. Hillier, B. Mazidian, J. Quintanilla, J. F. Annett, D. McK. Paul, G. Balakrishnan, and M. R. Lees, Phys. Rev. Lett. **112**, 107002 (2014).

[43] D. Singh, J. A. T. Barker, A. Thamizhavel, D. McK. Paul, A. D. Hillier, and R. P. Singh, Phys. Rev. B **96**, 180501(R) (2017).

[44] D. Singh, S. K. P., J. A. T. Barker, D. McK. Paul, A. D. Hillier, and R. P. Singh, Phys. Rev. B **97**, 100505(R) (2018).

[45] J. A. T. Barker, D. Singh, A. Thamizhavel, A. D. Hillier, M. R. Lees, G. Balakrishnan, D. McK. Paul, and R. P. Singh, Phys. Rev. Lett. **115**, 267001 (2015).

[46] T. Shang, M. Smidman, S. K. Ghosh, C. Baines, L. J. Chang, D. J. Gawryluk, J. A. T. Barker, R. P. Singh, D. McK. Paul, G. Balakrishnan, E. Pomjakushina, M. Shi, M. Medarde, A. D. Hillier, H. Q. Yuan, J. Quintanilla, J. Mesot, and T. Shiroka, Phys. Rev. Lett. **121**, 257002 (2018).

[47] M. S. Scheurer, D. F. Agterberg, and J. Schmalian, npj Quantum Mater. **2**, 9 (2017).

[48] M. S. Scheurer, Phys. Rev. B **93**, 174509 (2016).

[49] M. A. Khan, A. B. Karki, T. Samanta, D. Browne, S. Stadler, I. Vekhter, A. Pandey, P. W. Adams, D. P. Young, S. Teknowijoyo, K. Cho, R. Prozorov, and D. E. Graf, Phys. Rev. B **94**, 144515 (2016).

[50] D. Singh, M. S. Scheurer, A. D. Hillier, and D. T. Adroja, and R. P. Singh, Phys. Rev. B **102**, 134511 (2020).

[51] B. Li, C. Q. Xu, W. Zhou, W. H. Jiao, R. Sankar, F. M. Zhang, H. H. Hou, X. F. Jiang, B. Qian, B. Chen, A. F. Bangura and X. Xu, Sci. Rep. **8**, 651 (2018).

[52] A. D. Hillier, J. S. Lord, K. Ishida, and C. Rogers, Phil. Trans. R. Soc. A **377**, 20180064 (2019).

[53] P. Fischer, W. Hälg, L. Schlapbach, and K. Yvon, J. Less-Common Met. **60**, 1 (1978).

[54] A. Nakamura, F. Honda, Y. Homma, D. Li, K. Nishimura, M. Kakihana, M. Hedo, Takao Nakama, Y. Onuki and D. Aoki, J. Phys. Conf. Ser. **807**, 052012 (2017).

[55] H. Padamsee, J. E. Neighbor, and C. A. Shiffman, J. Low Temp. Phys. **12**, 387 (1973).

[56] F. Bouquet, Y. Wang, R. A. Fisher, D. G. Hinks, J. D. Jorgensen, A. Junod, and N. E. Phillips, Europhys. Lett. **56**, 856 (2001).

[57] M. Weber, A. Amato, F. N. Gygax, A. Schenck, H. Maletta, V. N. Duginov, V. G. Grebinnik, A. B. Lazarev, V. G. Olshevsky, V. Yu. Pomjakushin, S. N. Shilov, V. A. Zhukov, B. F. Kirillov, A. V. Pirogov, A. N. Ponomarev, and V. G. Storchak, S. Kapusta, and J. Bock, Phys. Rev. B **48**, 13022 (1993).

[58] A. Maisuradze, R. Khasanov, A. Shengelaya, and H. Keller, J. Phys.: Condens. Matter **21**, 075701 (2009).

[59] R. Khasanov, D. G. Eshchenko, D. Di Castro, A. Shengelaya, F. La Mattina, A. Maisuradze, C. Baines, H. Luetkens, J. Karpinski, S. M. Kazakov, and H. Keller, Phys. Rev. B **72**, 104504 (2005).

[60] E. H. Brandt, Phys. Rev. B **68**, 054506 (2003).

[61] B. S. Chandrasekhar and D. Einzel, Ann. Phys., Lpz. **505**, 535 (1993).

[62] R. Prozorov and R. W. Giannetta, Supercond. Sci. Technol. **19**, R41 (2006).

[63] R. S. Hayano, Y. J. Uemura, J. Imazato, N. Nishida, T. Yamazaki, and R. Kubo, Phys. Rev. B **20**, 850 (1979).

[64] G. M. Luke, Y. Fudamoto, K. M. Kojima, M. I. Larkin, J. Merrin, B. Nachumi, Y. J. Uemura, Y. Maeno, Z. Q. Mao, Y. Mori, H. Nakamura, and M. Sigrist, Nature (London) **394**, 558 (1998).

[65] A. Bhattacharyya, D. T. Adroja, J. Quintanilla, A. D. Hillier, N. Kase, A. M. Strydom, and J. Akimitsu, Phys. Rev. B **91**, 060503(R) (2015).

[66] V. Grinenko, R. Sarkar, K. Kihou, C. H. Lee, I. Morozov, S. Aswartham, B. Büchner, P. Chekhonin, W. Skrotzki, K. Nenkov, R. Hühne, K. Nielsch, S.-L. Drechsler, V. L. Vadimov,

[67] A. Ribak, R. Majlin Skiff, M. Mograbi, P. K. Rout, M. H. Fischer, J. Ruhman, K. Chashka, Y. Dagan and A. Kanigel, Sci. Adv. **6**, eaax9480 (2020).

[68] A. Maisuradze, W. Schnelle, R. Khasanov, R. Gumeniuk, M. Nicklas, H. Rosner, A. Leithe-Jasper, Yu. Grin, A. Amato, and P. Thalmeier, Phys. Rev. B **82**, 024524 (2010).

[69] J. Zhang, D. E. MacLaughlin, A. D. Hillier, Z. F. Ding, K. Huang, M. B. Maple, and L. Shu, Phys. Rev. B **91**, 104523 (2015).

[70] J. Zhang, Z. F. Ding, K. Huang, C. Tan, A. D. Hillier, P. K. Biswas, D. E. MacLaughlin, and L. Shu, Phys. Rev. B **100**, 024508 (2019).

[71] M. Sahakyan and V. H. Tran, Phys. Lett. A **384**, 126118 (2020).

[72] J. Garaud and E. Babaev, Phys. Rev. Lett. **112**, 017003 (2014).

[73] S. Maiti and A. V. Chubukov, Phys. Rev. B **87**, 144511 (2013).

[74] R. Balian and N. R. Werthamer, Phys. Rev. **131**, 1553 (1963).

[75] A. A. Golubov and I. I. Mazin, Phys. Rev. B **55**, 15146 (1997).

[76] M. S. Scheurer, Mechanism, symmetry and topology of ordered phases in correlated systems, Ph.D. thesis, Karlsruher Institut für Technologie (KIT), 2016.

[77] M. Hoyer, M. S. Scheurer, S. V. Syzranov, and J. Schmalian, Phys. Rev. B **91**, 054501 (2015).

[78] V. Grinenko, S. Ghosh, R. Sarkar, J.-C. Orain, A. Nikitin, M. Elender, D. Das, Z. Guguchia, F. Brückner, M. E. Barber, J. Park, N. Kikugawa, D. A. Sokolov, J. S. Bobowski, T. Miyoshi, Y. Maeno, A. P. Mackenzie, H. Luetkens, C. W. Hicks, and H.-H. Klauss, Nat. Phys. (2021), doi: 10.1038/s41567-021-01182-7.

[79] M. Tinkham, *Introduction to Superconductivity*, 2nd ed. (McGraw-Hill, New York, 1996).

[80] J. Garaud, A. Corticelli, M. Silaev, and E. Babaev, Phys. Rev. B **98**, 014520 (2018).

[81] Z. Fisk and G. W. Webb, Phys. Rev. Lett. **36**, 1084 (1976).

[82] H. Wiesmann, M. Gurvitch, H. Lutz, A. K. Ghosh, B. Schwarz, M. Strongin, P. B. Allen, and J. W. Halley, Phys. Rev. Lett. **38**, 782 (1977).

[83] G. Grimvall, *The Electron-Phonon Interaction in Metals* (North-Holland, Amsterdam, 1981).

[84] J. A. T. Barker, Muon studies of unconventional superconductors, Ph. D. thesis, University of Warwick, 2016.

[85] R. Samajdar and M. S. Scheurer, Phys. Rev. B **102**, 064501 (2020).